Check for updates

Accepted Article

Title: Drug design inspired by Nature: Crystallographic detection of auto-tailored protease inhibitor template

Authors: Flavio M. Gall, Deborah Hohl, David Frasson, Tobias Wermelinger, Peer R. E. Mittl, Martin Sievers, and Rainer Riedl

WILEY-VCH

COMMUNICATION

Drug design inspired by Nature: Crystallographic detection of auto-tailored protease inhibitor template

Flavio M. Gall,[a] Deborah Hohl,[a] David Frasson,[b] Tobias Wermelinger,[b] Peer R. E. Mittl,[c] Martin Sievers,[b] and Rainer Riedl*[a]

Abstract: *De novo* drug discovery is still a challenge in the search for potent and selective modulators of therapeutically relevant target proteins. Here, we disclose the unexpected discovery of a peptidic ligand **1** by X-ray crystallography, auto-tailored by the therapeutic target MMP-13 through partial self-degradation and the subsequent structure-based optimization to a highly potent and selective β-sheet peptidomimetic inhibitor derived from the endogenous tissue inhibitors of metalloproteinases (TIMPs). The incorporation of non-proteinogenic amino acids in combination with a cyclization strategy proved to be key for the *de novo* design of TIMP peptidomimetics. The optimized cyclic peptide **4** (ZHAWOC7726) is membrane permeable with an IC_{50} of 21 nM for MMP-13 and an attractive selectivity profile with respect to a polypharmacology approach including the anti-cancer targets MMP-2 (IC_{50}: 170 nM) and MMP-9 (IC_{50}: 140 nM).

Peptides are major components for the modulation of important biological processes from reproduction, signaling, regulation to cell death.[1,2] The application of peptides as drug molecules has been limited due to their inherently low stability, low membrane permeability and high *in vivo* clearance.[3] However, the high specificity, chemical diversity and low toxicity (nontoxic metabolites and no accumulation) of peptides, matched with more drug like properties, caught the attention of the pharmaceutical industry.[3–5] Several linear and cyclic peptides in particular penetrate membranes and are even orally available.[6–8] With 60 US Food and Drug Administration (FDA)-approved peptide therapeutics on the market[9] and currently over 150 in active clinical development,[10] a clear evolvement of this class and a paradigm shift in the pharmaceutical industry is ongoing.[4,11,12]

The matrix metalloproteinases (MMPs) are a family of over twenty zinc-dependent endopeptidases involved in degrading extracellular matrix (ECM) proteins. They are involved in many serious diseases like cancer, osteoarthritis, inflammatory processes, to name a few.[13–17] MMP-13 is among others overexpressed in osteoarthritic cartilage and preferentially cleaves collagen-II.[18] The tissue inhibitors of metalloproteinases (TIMPs) are a group of four specific endogenous protein inhibitors for MMPs. Recent studies showed a clear need for specific small molecule MMP inhibitors for clinical application.[19] In this study, we developed potent and selective cyclic β-sheet TIMP peptidometics based on an auto-tailored peptidic inhibitor template.

During co-crystallization experiments with MMP-13 and small molecule inhibitors,[20–22] we made a surprising discovery. The 1.71 Å resolution crystal structure of MMP-13 revealed that despite the high affinity of the small molecule inhibitor it was not resolved in the electron density map (coordinates have been deposited at the PDB under 6HV2, Table S6). Instead, the difference electron density suggested the binding of a pentapeptide into the prime site of MMP-13. The high resolution and the quality of the map allowed the assignment of the sequence Ile-Met-Ile to the three *N*-terminal residues of the peptide. This sequence suggested that the bound pentapeptide is a self-degradation fragment that corresponds to residues Ile163-Phe167 of MMP-13 (UniProtKB: P45452[23]). Subsequent refinement rounds proved that the sequence Ile-Met-Ile-Ser-Phe **1** perfectly matches the electron density. The peptide ligand occupies the prime site of the catalytic groove of MMP-13 as shown in Figure 1.

The peptide ligand adopts a β-sheet conformation that aligns anti-parallel to the central β-sheet of MMP-13 and closes the gap to the loop formed by residues 242 to 244.[24] The *N*-terminal amine is located at the catalytic zinc and forms hydrogen bonds to Glu223. The main chain oxygen and nitrogen atoms of Ile163 ligate the catalytic zinc ion and the side chain of Met164 occupies the S1' pocket of MMP-13. In solution, the hydrophobic side chains of Ile163 and Ile165 are solvent exposed, whereas in the crystal lattice this hydrophobic patch is involved in a crystal contact, covering the side chains of Met240*, Phe241* and Ile243* from the symmetry mate. The hydrophobic nature of this contact is probably important to stabilize the MMP-13/IMISF complex in the crystal lattice. Residue Phe167 does not form any specific interactions and is just weakly defined in the electron density map. Enzyme-product complexes are usually not very stable in order to preserve the activity of the enzyme. In this case, several circumstances may have stabilized the discovered complex such as the lipophilic crystal contact with Met240*, Phe241* and Ile243* but also the high pH of 9.4 during the crystallization experiments. Here, the uncharged *N*-terminal amine strongly coordinates to the catalytic zinc ion and lowers the proteolytic activity of the protease, thus preventing the peptide from further degradation.

The exciting discovery of the auto-tailored pentapeptide **1** in combination with the structural comparison with TIMPs provided the basis for structure-based *de novo* design of TIMP peptidomimetics. The four TIMPs 1 to 4 are capable of inhibiting all MMPs but the efficacy of MMP inhibition varies for each

[a]   F. M. Gall, D. Hohl, Prof. Dr. R. Riedl
      Institute of Chemistry and Biotechnology, Center of Organic and
      Medicinal Chemistry
      ZHAW Zurich University of Applied Sciences
      Einsiedlerstr. 31, 8820 Wädenswil, Switzerland
      E-mail: rainer.riedl@zhaw.ch
[b]   D. Frasson, T. Wermelinger, Prof. Dr. M. Sievers
      Institute of Chemistry and Biotechnology, Center of Molecular
      Biology
      ZHAW Zurich University of Applied Sciences
      Einsiedlerstr. 31, 8820 Wädenswil, Switzerland
[c]   PD Dr. P. R. E. Mittl
      Department of Biochemistry
      University of Zurich, Winterthurerstr. 190, 8057 Zürich, Switzerland

      Supporting information for this article is given via a link at the end of
      the document
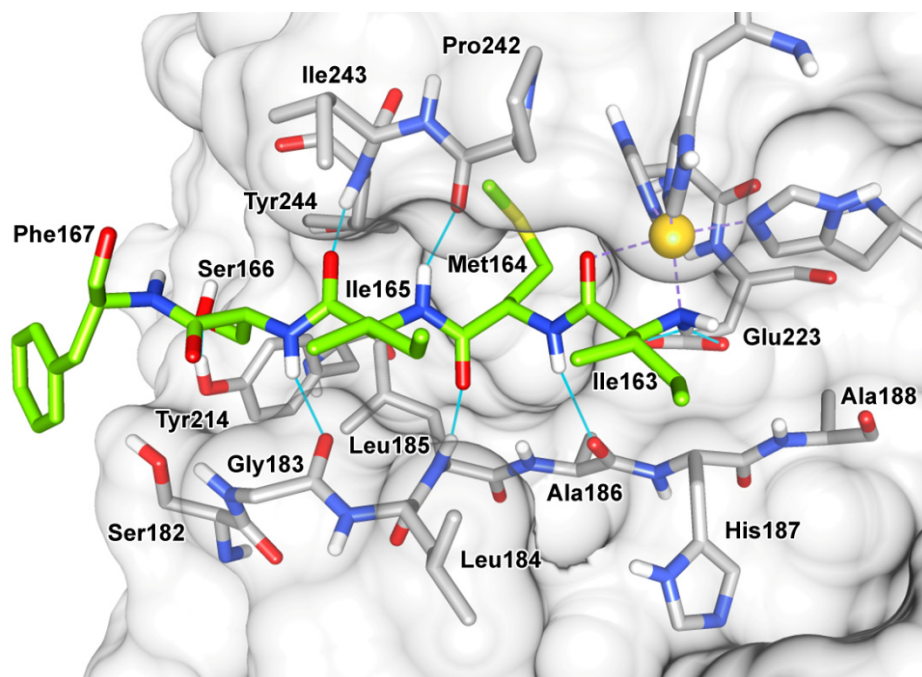
COMMUNICATION

Figure 1. MMP-13/pentapeptide **1** X-ray co-crystal structure. The pentapeptide H-Ile-Met-Ile-Ser-Phe-OH **1** (carbons in green) forms an anti-parallel β-sheet motive with Ser182-Ala188. The *N*-terminal amine is located at the catalytic zinc ion (Zn^{2+} ion as golden sphere) and is engaged in hydrogen bonds to Glu223.
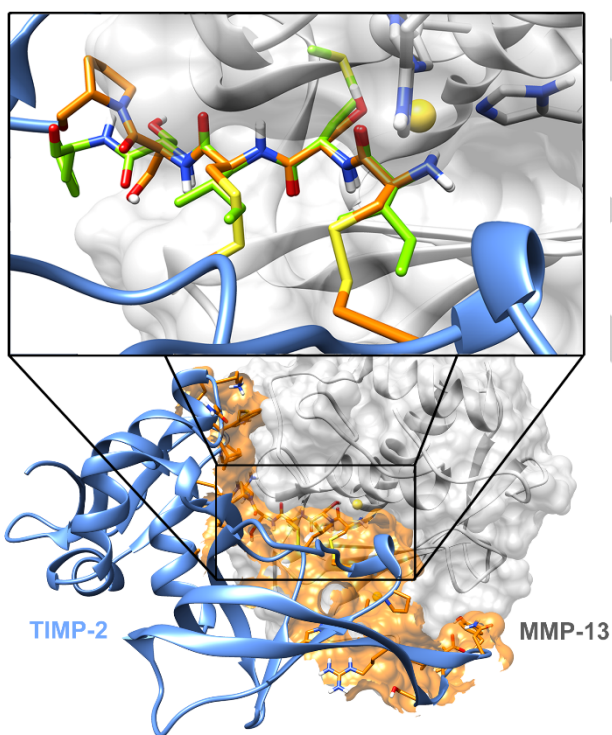

Figure 2. TIMP-2 (ribbon in blue) binds to the catalytic groove of MMP-13 (PDB: 2E2D[25]) and covers a large surface within a distance of 5 Å (displayed in orange). The magnified section shows the five *N*-terminal amino acids (carbons in orange) in an overlay with the pentapeptide **1** (carbons in green, Zn^{2+} ion as golden sphere).

TIMP.[26] They bind to the active site cleft of MMPs[25,27] as shown in Figure 2 and cover a surface of about 1300 Å^2.[2,28] Although the sequence is completely different, peptide **1** forms very similar backbone interactions compared to the *N*-terminal sequence of

bound TIMPs (Figure 2). Consequently, these interactions were conserved during the design process.

The pentapeptide **1** offered many options for variations: Besides the optimal length and sequence of the peptide template, two other features were targeted for the *de novo* design of TIMP peptidomimetics.

I) The sidechain of the second amino acid is crucial for the binding of TIMPs[29] and represents an excellent branching position to reach into the S1' pocket (Figure 3). In MMP-13, this pocket forms a characteristically extended straight tunnel surrounded by nonpolar amino acids. Ligands can potentially form π-π interactions with His222 or edge to face interactions with Tyr244, Phe241 or Phe252. The S1' pocket varies between different MMPs with respect to size, composition and flexibility. In MMP-13, it is relatively rigid compared to other MMPs, and MMP-13 has the largest S1' pocket within the MMP family.[30] Co-crystal structures with small organic molecules show for MMP-13 a preference for linear nonpolar groups like biphenyl moieties.[31–33] In contrast, MMPs with a smaller S1' pocket cannot accommodate comparable groups or must undergo conformational changes.[34] In MMP-13, this pocket needs no or little structural adaption to accommodate such groups.[30, 34] Non-proteinogenic amino acids can integrate such fragments into the peptide to achieve selectivity within the MMP family.

II) The macrocyclisation in TIMPs *via* two disulfide bridges was transferred to the peptidomimetic using a side chain to side chain cyclisation strategy between the two isoleucine residues. This side chain cyclization rigidifies the peptidic inhibitor and preforms the conformation of single stranded β-sheet mimetics.[35–37]

Several non-proteinogenic amino acids with linear, nonpolar side chains as S1' pocket binders or anchor groups for cyclisation reactions were synthesized (Scheme S1) and employed in automated microwave-assisted solid phase peptide synthesis (SPPS). Ring closing metathesis as well as a copper(I)-catalyzed alkyne-azide cycloaddition strategy were applied to the protected resin bound linear peptide precursor (Schemes 1 and S2).[38]

The co-crystallized auto-tailored linear pentapeptide **1** showed an IC$_{50}$ value of 52 μM against MMP-13. In order to increase the inhibitory potency and selectivity, a structure activity relationship was established by modifying the amino acid side chains binding into the S1' pocket. Here, biphenyl fragments proved to be beneficial and the *p*-trifluoromethoxy substituted derivative was the most potent derivative (Table S1). Slightly bended moieties such as biphenyl ethers showed significantly lower potencies compared to linear biphenyl groups. This can be rationalized by steric constraints in the linear S1' pocket. To determine the optimal length of the peptide template, shorter peptides were generated and an Ala-scan was performed (Table S2). All shorter

Accepted Manuscript
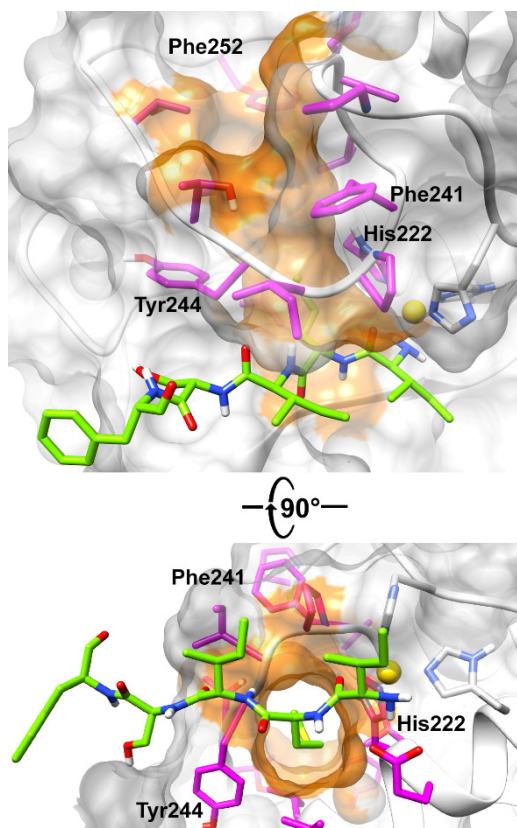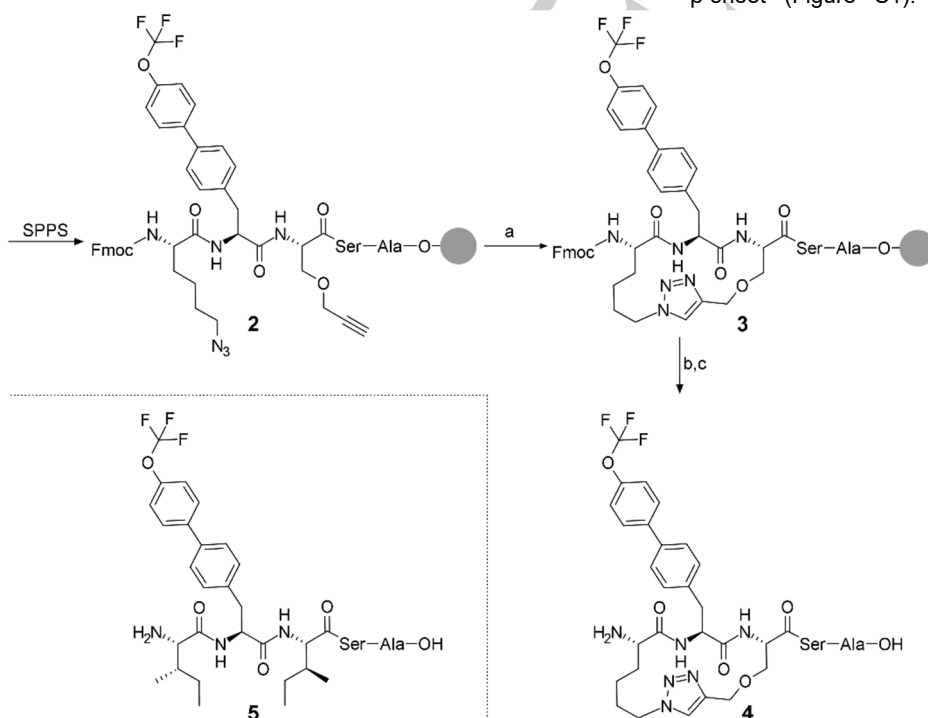
COMMUNICATION

Figure 3. MMP-13/pentapeptide **1** X-ray co-crystal structure. The S1' pocket is highlighted in orange, Zn^{2+} ion as golden sphere. The flanking amino acids (carbons in magenta) form a hydrophobic tunnel. This conserved tunnel provides enough space for larger nonpolar groups.

peptides were less potent and an exchange with alanine was only tolerated at the fifth position. The phenylalanine side chain points towards the solvent. This hydrophobic group was exchanged by an alanine in order to decrease the molecular weight and to increase the polarity.

The co-crystal structure in Figure 1 indicates coordination of the *N*-terminal amino group to the positively charged catalytic zinc ion and hydrogen bonds to the negatively charged side chain of Glu223. Within this network of interactions, manipulations on the *N*-terminus, such as removing the amino group or the *N*-methylation, were well tolerated as shown by the IC_{50} values of the resulting peptides (Table S3). The pKa values of *N*-terminal amino groups in proteins have documented values between 6.8 and 9.1 with an average of 7.7 ± 0.5.[39] We assume the *N*-terminus of **1** is unprotonated in the crystal structure, because the crystallization experiment was performed at pH 9.4. Hence, the lone electron pair of the *N*-terminal nitrogen is available for the coordination of the Zn^{2+} ion. The Zn^{2+}-N distance in the MMP13/**1** complex is 2.1 Å, which is similar to distances seen in TIMP/MMP complexes that were crystallized at physiological pH (2E2D[25] at pH 6.5 and 2J0T[40] at pH 7.5).

We decided to keep the amino group in the following molecules as solubility mediator because aqueous solubility is a major issue in drug development projects and amino groups allow beneficial salt formation during drug formulation.

A cyclisation strategy between the sidechains of the first and third amino acid of the linear peptidic core structure was used to mimic the macrocyclisation *via* two disulfide bridges in TIMPs (Figure 2). Modelling experiments indicated that the ring size of the cyclic peptide should be at least 15 atoms. Smaller rings tend to tear the backbone out of the catalytic groove and break up the β-sheet (Figure S1). Among the synthesized cyclic TIMP peptidomimetics, the 17-membered triazole containing derivative **4** (ZHAWOC7726, Scheme 1) showed more than 100-fold improvement of inhibitory potency (IC_{50} of 21 nM, Table S4) compared to its linear counterpart **5**. This affinity improvement can be rationalized by beneficial preorganization of the inhibitor through macrocyclization.[35]

To get better insight into the interactions of the superior macrocycle **4**, the TIMP peptidomimetic was docked to MMP-13 using the in-house generated original co-crystal structure (PDB: 6HV2). Figure 4 was generated with the modeling platform tool MOE (molecular operating environment)[41] and represents all targeted interactions. The non-proteinogenic amino acid side chain binds into the S1' pocket and the macrocycle shields and rigidifies the β-sheet forming peptidic inhibitor scaffold.

The cyclic peptide **4** was tested against different MMPs with respect to

Scheme 1. Solid phase peptide synthesis of the cyclic peptidomimetic **4** *via* on-resin cyclization and depiction of the linear counterpart **5**. (a) DMSO, H_2O, CuBr, sodium ascorbate, 2,6-lutidine, DIPEA, rt, 16 h; (b) DMF, piperidine, rt, 2 x 10 min; (c) TFA, H_2O, triisopropylsilane, rt, 2 h, 8 % (11 steps).
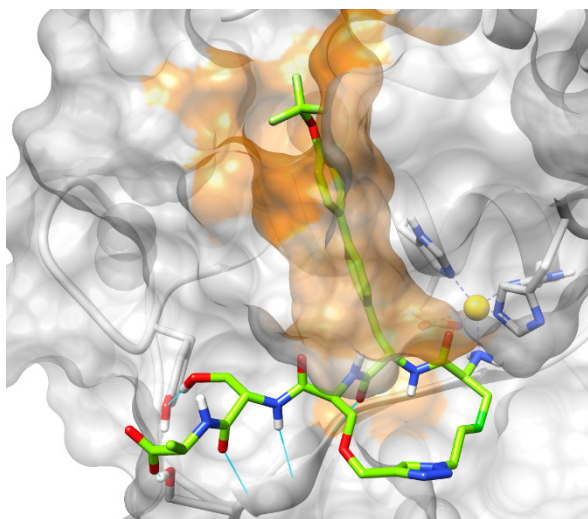
COMMUNICATION

Figure 4. Potent and selective macrocyclic TIMP peptidomimetic **4** (carbons in green, Zn^{2+} ion as golden sphere) modelled into the MMP-13/**1** X-ray co-crystal structure.

its inhibitory potency in order to determine the selectivity profile (Table S5). The inhibitor **4** shows an excellent selectivity profile against MMPs with a small S1' pocket because of the bulky non-proteinogenic amino acid moiety. In accordance with our design strategy, the TIMP peptidomimetic **4** inhibits the structurally closely related MMP family members MMP-2 (IC_{50} = 170 nM), MMP-9 (IC_{50} = 140 nM) and MMP-12 (IC_{50} = 74 nM) with comparable potency because they share a S1' pocket of similar volume.[42–44] As MMP-2 and MMP-9 are as well as MMP-13 validated anti-cancer targets,[13] this represents a very attractive inhibition profile for a polypharmacology approach toward the treatment of cancer by MMP inhibition. Noteworthy, the macrocyclic peptidic inhibitor **4** exhibits excellent selectivity over MMP-10 although this has also a deep S1' pocket but with different amino acid composition.[22,30,33,45] Ilomastat was used as positive control for all MMP inhibition assays (Table S7). This potent and broad-spectrum MMP inhibitor represents a peptidomimetic containing a hydroxamic acid as zinc-binding group. This zinc-binding group leads to very strong inhibitory potency (subnano molar IC_{50} values across a wide range of MMPs, including several antitargets) but caused fatal problems in clinical studies including poor oral bioavailability and severe side effects due to a lack of selectivity. We used ilomastat because it shares the peptidic nature with our TIMP peptidomimetic and this type of inhibitors has been intensively studied in the past.[46–48] The macrocyclic peptidic inhibitor **4** contains no problematic hydroxamic acid as zinc-binding group but still shows nano molar inhibition and a very appealing selectivity profile.

Aqueous solubility, parallel artificial membrane permeability assays (PAMPA) and stability in human liver microsomes were measured for **4** and the linear counterpart **5**. The aqueous solubility of the cyclic version is significantly higher (522 µM for **4**, versus 27 µM for **5**). The cLogP values indicate higher polarity for the cyclic peptide as an explanation for the higher solubility (cLogP values in Table S4). Fortunately, the PAMPA results for the blood-brain barrier (BBB) and gastrointestinal tract (GIT) show high permeability for both the linear and the cyclic version (**5**: $LogP_{app}$(BBB) = -4.5 and $LogP_{app}$(GIT) = - 4.2 [10^{-6} cm/s]; **4**:

$LogP_{app}$(BBB) -4.7 and $LogP_{app}$(GIT) = - 4.6 [10^{-6} cm/s]). In addition, both peptides show good stability in a human liver microsome assay. Here, the cyclic TIMP peptidomimetic **4** showed better performance than the linear counterpart did (**4**: half-life = 45.2 min; **5**: half-life = 39.1 min).

In conclusion, we utilized X-ray crystallographic data of an enzyme-product complex for the structure-based *de novo* design of TIMP peptidomimetics. The interplay between surprising crystallographic data, a suitable synthetic cyclization strategy and the employment of non-proteinogenic amino acids as crucial binding fragments were key factors in this study. In contrast to traditional screening campaigns within libraries of synthetic molecules and natural products, we started with a natural ligand that has been produced by the biological target through partial self-degradation. We were able to convert this low-affinity binder into a potent and selective cyclic membrane permeable TIMP peptidomimetic targeting MMP-2, MMP-9 and MMP-13 suitable for polypharmacology approaches in cancer therapy. This method bears great potential for initiating drug discovery projects by high-throughput crystallization in the field of protease targets and provides an additional tool to our hit and subsequent lead generation techniques.

Acknowledgements

[1] T. A. Hill, N. E. Shepherd, F. Diness, D. P. Fairlie, *Angew. Chem. - Int. Ed.* **2014**, *53*, 13020–13041; T. A. Hill, N. E. Shepherd, F. Diness, D. P. Fairlie, *Angew. Chem.* **2014**, *126*, 13234–13257.

[2] M. R. Arkin, Y. Tang, J. A. Wells, *Chem. Biol.* **2014**, *21*, 1102–1114.

[3] T. A. F. Cardote, A. Ciulli, *ChemMedChem* **2016**, *11*, 787–794.

[4] L. Otvos, J. D. Wade, *Front. Chem.* **2014**, *2*, 8–11.

[5] A. Tapeinou, M. T. Matsoukas, C. Simal, T. Tselios, *Biopolymers* **2015**, *104*, 453–461.

[6] D. S. Nielsen, N. E. Shepherd, W. Xu, A. J. Lucke, M. J. Stoermer, D. P. Fairlie, *Chem. Rev.* **2017**, *117*, 8094–8128.

[7] G. B. Santos, A. Ganesan, F. S. Emery, *ChemMedChem* **2016**, *11*, 2245–2251.

[8] W. M. Hewitt, S. S. F. Leung, C. R. Pye, *J. Am. Chem. Soc.* **2015**, *137*, 715–721.

[9] K. Fosgerau, T. Hoffmann, *Drug Discov. Today* **2015**, *20*, 122–128.

[10] J. L. Lau, M. K. Dunn, *Bioorganic Med. Chem.* **2018**, *26*, 2700–2707.

[11] N. Tsomaia, *Eur. J. Med. Chem.* **2015**, *94*, 459–470.

[12] T. Uhlig, T. Kyprianou, F. G. Martinelli, C. A. Oppici, D. Heiligers, D.

COMMUNICATION

Hills, X. R. Calvo, P. Verhaert, *EuPA Open Proteomics* **2014**, *4*, 58–69.

[13] C. M. Overall, O. Kleifeld, *Nat. Rev. Cancer* **2006**, *6*, 227–239.

[14] L. M. Coussens, *Science.* **2002**, *295*, 2387–2392.

[15] J. F. Fisher, S. Mobashery, *Cancer Metastasis Rev.* **2006**, *25*, 115–136.

[16] R. E. Vandenbroucke, C. Libert, *Nat. Rev. Drug Discov.* **2014**, *13*, 904–927.

[17] M. Egeblad, Z. Werb, *Nat. Rev. Cancer* **2002**, *2*, 161–174.

[18] S. Amar, L. Smith, G. B. Fields, *Biochim. Biophys. Acta - Mol. Cell Res.* **2017**, *1864*, 1940–1951.

[19] X. W. Xie, R. Z. Wan, Z. P. Liu, *ChemMedChem* **2017**, *12*, 1157–1168.

[20] T. Fischer, R. Riedl, *ChemistryOpen* **2017**, *6*, 192–195.

[21] J. Lanz, R. Riedl, *ChemMedChem* **2015**, *10*, 451–454.

[22] N. Senn, M. Ott, J. Lanz, R. Riedl, *J. Med. Chem.* **2017**, *60*, 9585–9598.

[23] A. Bateman, M. J. Martin, C. O'Donovan, M. Magrane, E. Alpi, R. Antunes, B. Bely, M. Bingley, C. Bonilla, R. Britto, *et al.*, *Nucleic Acids Res.* **2017**, *45*, D158–D169.

[24] W. Bode, R. Huber, *Eur. J. Biochem.* **1992**, *204*, 433–451.

[25] K. Maskos, R. Lang, H. Tschesche, W. Bode, *J. Mol. Biol.* **2007**, *366*, 1222–1231.

[26] V. Arpino, M. Brock, S. E. Gill, *Matrix Biol.* **2015**, *44–46*, 247–254.

[27] F.-X. Gomis-Ruth, K. Maskos, M. Betz, A. Bergner, R. Huber, K. Suzuki, N. Yoshida, H. Nagase, K. Brew, G. P. Bourenkov, *et al.*, *Nature* **1997**, *389*, 77–81.

[28] K. Maskos, W. Bode, *Mol. Biotechnol.* **2003**, *25*, 241–266.

[29] B. Stratmann, M. Farr, H. Tschesche, *FEBS Lett.* **2001**, *507*, 285–287.

[30] B. Fabre, A. Ramos, B. De Pascual-Teresa, *J. Med. Chem.* **2014**, *57*, 10205–10219.

[31] D. P. Becker, T. E. Barta, L. J. Bedell, T. L. Boehm, B. R. Bond, J. Carroll, C. P. Carron, G. A. Decrescenzo, A. M. Easton, J. N. Freskos, et al., *J. Med. Chem.* **2010**, *53*, 6653–6680.

[32] R. A. Tommasi, S. Weiler, L. W. Mcquire, O. Rogel, M. Chambers, K. Clark, J. Doughty, J. Fang, V. Ganu, J. Grob, *et al.*, *Bioorganic Med. Chem. Lett.* **2011**, *21*, 6440–6445.

[33] L. Devel, F. Beau, M. Amoura, L. Vera, E. Cassar-Lajeunesse, S. Garcia, B. Czarny, E. A. Stura, V. Dive, *J. Biol. Chem.* **2012**, *287*, 26647–26656.

[34] B. Lovejoy, A. R. Welch, S. Carr, *Nat. Struct. Biol.* **1999**, *6*, 217–21.

[35] W. A. Loughlin, J. D. A. Tyndall, M. P. Glenn, D. P. Fairlie, *Chem. Rev.* **2004**, *104*, 6085–6117.

[36] R. C. Reid, M. J. Kelso, M. J. Scanlon, D. P. Fairlie, *J. Am. Chem. Soc.* **2002**, *124*, 5673–5683.

[37] M. P. Glenn, D. P. Fairlie, *Mini Rev. Med. Chem.* **2002**, *2*, 433–445.

[38] Y.-W. Kim, T. N. Grossmann, G. L. Verdine, *Nat. Protoc.* **2011**, *6*, 761–71.

[39] G. R. Grimsley, J. M. Scholtz, C. N. Pace, *Protein Sci.* **2009**, *18*, 247–251.

[40] S. Iyer, S. Wei, K. Brew, K. R. Acharya, *J. Biol. Chem.* **2007**, *282*, 364–371.

[41] *Molecular Operating Environment (MOE)*, 2013.08; Chemical Computing Group ULC, Montreal, QC, Canada, **2018**.

[42] Y. Feng, J. J. Likos, L. Zhu, H. Woodward, G. Munie, J. J. McDonald, A. M. Stevens, C. P. Howard, G. A. De Crescenzo, D. Welsch, *et al.*, *Biochim. Biophys. Acta - Proteins Proteomics* **2002**, *1598*, 10–23.

[43] A. Tochowicz, K. Maskos, R. Huber, R. Oltenfreiter, V. Dive, A. Yiotakis, M. Zanda, W. Bode, P. Goettig, *J. Mol. Biol.* **2007**, *371*, 989–1006.

[44] R. Lang, A. Kocourek, M. Braun, H. Tschesche, R. Huber, W. Bode, K. Maskos, *J. Mol. Biol.* **2001**, *312*, 731–742.

[45] J. Batra, J. Robinson, A. S. Soares, A. P. Fields, D. C. Radisky, E. S. Radisky, *J. Biol. Chem.* **2012**, *287*, 15935–15946.

[46] D. Grobelny, L. Poncz, R. E. Galardy, *Biochemistry* **1992**, *31*, 7152–7154

[47] M. Hidalgo, S. G. Eckhardt, *JNCI J. Natl. Cancer Inst.* **2001**, *93*, 178–193.

[48] B. Fingleton, *Curr. Pharm. Des.* **2007**, *13*, 333–346.

[49] E. F. Pettersen, T. D. Goddard, C. C. Huang, G. S. Couch, D. M. Greenblatt, E. C. Meng, T. E. Ferrin, *J. Comput. Chem.* **2004**, *25*, 1605–1612.

WILEY-VCH

COMMUNICATION

COMMUNICATION

Closing the circle: The crystallographic discovery of a peptide generated through partial self-degradation of the therapeutic target paves the way for the *de novo* generation of a potent and selective cyclic peptidomimetic of the endogenous tissue inhibitors of metalloproteinases (TIMPs).
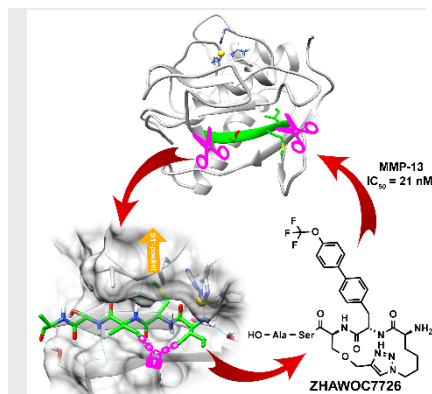
Flavio M. Gall, Deborah Hohl, David Frasson, Tobias Wermelinger, Peer R. E. Mittl, Martin Sievers, Rainer Riedl*

Page No. – Page No.
Drug design inspired by Nature: Crystallographic detection of auto-tailored protease inhibitor template